Science & Technology Development Journal 2024, 27(2):3453-3462

Open Access Full Text Article

Research article

Low-cost synthesis of α-Fe_2O_3 nanorods for photocatalytic application

Hoai Nhan Luong[1,2], Le Ngoc Thu Nguyen[1,2], Tan Muon Dinh[1,2], Nguyen Dan Nhi Huynh[1,2], Le Thai Duy[1,2], Cong Khanh Tran[1,2], Vinh Quang Dang[1,2,*]

ABSTRACT

Introduction: α-Fe_2O_3 nanorods (α-Fe_2O_3 NRs), also known as hematite, possess a narrow band gap, high chemical stability, extensive surface area, controllable size, and outstanding photoelectric properties. These attributes make hematite a promising material for various applications, including gas sensors, optical sensors, and notably, photocatalysis. In previous studies, α-Fe_2O_3 nanorods were synthesized using various processes. However, these processes involve extensive use of precursors, are expensive, and time-consuming, and have negative impacts on the environment. Hence, this investigation introduces an uncomplicated, efficient, and high-precision hydrothermal process for synthesizing α-Fe_2O_3 nanorods (α-Fe_2O_3 NRs). **Methods**: We utilized a short-term hydrothermal process to synthesize α-Fe_2O_3 nanorods. Characterization of the nanorods involved XRD, VESTA, Raman, SEM, and EDX to examine their morphology and structure, with UV-Vis spectroscopy used to determine their absorption spectra. The photocatalytic efficiency of the α-Fe_2O_3 nanorods was assessed by their ability to degrade methylene blue dye at a concentration of 2.5 ppm. **Results**: VESTA simulations and XRD patterns confirmed that the α-Fe_2O_3 nanorods have a rhombohedral crystal structure and belongs to space group $R\bar{3}c$. The optical bandgap was determined to be 2.2 eV through calculations using Tauc's method. Through scanning electron microscopy (SEM), the average length and diameter of the α-Fe_2O_3 NRs were determined to be 415 nm and 110 nm, respectively. The photocatalytic capacity for degrading methylene blue (concentration of 2.5 ppm) was 55%. **Conclusion**: This exploration of the fundamental characteristics of α-Fe_2O_3 NRs offers deeper insights into the properties of nanorod-structured hematite materials. Moreover, the synthesis of α-Fe2O3 NRs using this hydrothermal method addresses several previously identified challenges, thereby contributing to broadening the potential applications of α-Fe_2O_3 NRs across various fields in the future.

Key words: α-Fe2O3 nanorods, hematite, photocatalyst, VESTA, simulation

[1]*Faculty of Materials Science and Technology, University of Science, Ho Chi Minh City, Vietnam*

[2]*Vietnam National University, Ho Chi Minh City, Vietnam*

Correspondence

Vinh Quang Dang, Faculty of Materials Science and Technology, University of Science, Ho Chi Minh City, Vietnam

Vietnam National University, Ho Chi Minh City, Vietnam

Email: vinhquangntmk@gmail.com

History

- Received: 2024-03-30
- Accepted: 2024-05-31
- Published Online: 2024-6-30

DOI :

https://doi.org/10.32508/stdj.v27i2.4289

INTRODUCTION

In recent decades, the synthesis of one-dimensional (1D) nanostructures has garnered significant attention and extensive research across various fields due to their unique physical and chemical properties[1]. Additionally, the morphological diversity of one-dimensional nanostructures offers numerous advantages for various applications. For example, nanowires possess a high surface area-to-volume ratio, low defect density, and excellent optical conductivity, making them suitable for various applications, such as nanobiosensors, chemical sensors, gas sensors, and electrochemical sensors[2]. Due to their high specific surface area, nanotube structures can serve as frameworks or containers for other materials that can be applied in fuel cells, photocatalytic systems, energy storage, gas sensors, etc.,[3]. One particularly special and easily fabricated form of the 1D nanostructure is nanorods, which are characterized by large surface areas, easily controllable dimensions, and excellent optoelectronic properties. Nanorods have numerous important applications in light-emitting diodes (LEDs), light sensors, photocatalysis, gas sensors, biosensors, etc,.[4] Among the various types of 1D materials, α-Fe_2O_3 nanorods, also known as hematite, stand out due to their narrow band gap (approximately 2.2 eV), chemical stability, and nontoxic nature[5]. This makes hematite a highly significant material in numerous fields, such as magnetic applications[6,7], gas sensors[8], lithium-ion batteries[9], drug delivery technology[10], and particularly photocatalysis[11–14]. α-Fe_2O_3 nanorods have been synthesized using various physical and chemical methods, such as sol-gel methods[15], hydrothermal methods[16], vacuum thermal evaporation methods[17], green chemistry methods[18], and micelle methods[19]. However, physical methods often require expensive equipment and complex procedures, leading to limitations in

Cite this article : Luong H N, Nguyen L N T, Dinh T M, Huynh N D N, Duy L T, Tran C K, Dang V Q. **Low-cost synthesis of α-Fe_2O_3 nanorods for photocatalytic application**. *Sci. Tech. Dev. J.* 2024; 27(2):3453-3462.

practical applications hence, chemical methods are usually preferred. Among them, the hydrothermal method has become the preferred choice for α-Fe_2O_3 nanorod synthesis due to its low cost, simple synthesis process, and high efficiency compared to other methods. Despite its numerous advantages, hydrothermal synthesis still faces some challenges due to the use of multiple toxic precursors and prolonged reaction times, which can have negative environmental impacts. This can be observed in some previous studies. For instance, *Gajendra and colleagues* conducted a hydrothermal process for up to 36 hours, with an additional 3 hours required to obtain α-Fe_2O_3 nanorods using precursors such as diammonium phosphate and iron (III) chloride hexahydrate[20]. Additionally, the research group led by *Suyuan Zeng* synthesized α-Fe_2O_3 nanorods using a hydrothermal method with a total reaction time of 20 hours, employing sodium sulfite and iron(II) sulfate as precursors[21]. Furthermore, by utilizing iron(III) nitrate nonahydrate and sodium hydroxide for a 12-hour hydrothermal process, *Guo-Ying Zhang and colleagues* successfully synthesized α-Fe_2O_3 nanorods for photocatalytic applications[22].

In addition to the challenges related to the use of multiple precursors and long synthesis times, most research on photocatalysis only utilizes α-Fe_2O_3 nanorods (NRs) as a supporting material combined with other substances, such as cadmium oxide nanoparticles[12], cadmium sulfide nanoparticles[23], chromium dopants[13], or hybridization with reduced graphene oxide (rGO)[24]. This inadvertently blurs the distinctive properties of α-Fe_2O_3 NRs in photocatalysis, significantly impacting the optimization and enhancement of material structures to achieve maximum performance for future studies. Therefore, in this study, we focused on developing a simple hydrothermal process that saves time and utilizes fewer precursors to synthesize α-Fe_2O_3 nanorods. Additionally, the properties of the hematite material are examined and clearly presented through a combination of experimental work and simulation calculations. Furthermore, the photocatalytic capability of the α-Fe_2O_3 NRs was investigated through the degradation of methylene blue (MB) dye. With this method, this study not only provides a clearer understanding of the material but also partially addresses some of the abovementioned challenges, thereby contributing to expanding the potential applications of α-Fe_2O_3 nanorods in various fields in the future, both generally and particularly in the field of photocatalysis.

MATERIALS-METHODS

Chemical materials

The chemicals used in this experiment included iron(III) chloride hexahydrate ($FeCl_3 \cdot 6H_2O$, 99%, SigmaAldrich, USA), sodium nitrate ($NaNO_3$, 99%, SigmaAldrich, USA), and methylene blue (82%, SigmaAldrich, USA).

Characteristics

The surface morphology and density of the nanorods were examined using scanning electron microscopy (SEM, Hitachi S-4800). The crystalline structure of the α-Fe_2O_3 nanorods was observed via X-ray diffraction (XRD) performed on a D8 Advance-Bruker X-ray diffractometer operating at 40 kV and 100 mA with a Cu/Kα radiation source (λ = 0.154 nm). The optical properties of the nanorods were determined through UV–Vis spectroscopy (JASCO V670). Raman spectra were recorded using a Raman spectrometer (Xplora One, HORIBA) with an excitation wavelength of 532 nm, a power of 5 mW, a 10× objective, and an acquisition time adjusted to 15 seconds per spectrum. 3D structural models and XRD patterns based on computational simulations of α-Fe_2O_3 nanorods were generated using VESTA software (Visualization for Electronic Structural Analysis).

The photocatalytic efficiency of the α-Fe_2O_3 nanorods (NRs) was assessed by their ability to degrade methylene blue (MB) dye. The sample, with a size of 2 cm × 2 cm of α-Fe_2O_3 thin film, was added to 20 mL of the 2.5 ppm MB solution and then stirred evenly in the dark for 2 hours to ensure adsorption equilibrium. Subsequently, the sample was irradiated under visible light for 8 hours. The illumination source was a visible light lamp, equivalent to 1 sun, and a cooling fan was utilized to maintain the ambient temperature. The absorbance spectra of the MB solution were recorded at 2-hour intervals.

Fabrication processes

The synthesis of the α-Fe_2O_3 nanorods followed a hydrothermal method similar to that used in *Dong Chen's* study[25]. Initially, a solution containing $FeCl_3 \cdot 6H_2O$ (0.15 M) and $NaNO_3$ (1 M) with a total volume of 10 mL was prepared at room temperature. Once the precursors were completely dissolved in the solution, the mixture was transferred to a 25 mL Teflon-lined autoclave. Subsequently, a clean silicon substrate was placed inside the autoclave, which was then placed in an oven at 100 °C for 4 hours to

form FeOOH nanorods. Next, the sample was washed multiple times with deionized water and ethanol to remove impurities. Finally, the FeOOH sample was transferred to a furnace and annealed at 550 °C for 2 hours to convert it into α-Fe_2O_3 nanorods.

RESULTS

The simulated structure of α-Fe_2O_3 is depicted in Figure 1. Hematite possesses a rhombohedral crystal structure and belongs to the space group $R\bar{3}c$[26]. In each primitive cell, there are two formula units (a_{rh} = 5.427 Å; a = 55.3) (Figure 1a), whereas the unit cell contains six formula units (a = b = 5.034 Å; c = 13.75 Å) (Figure 1b)[27]. Furthermore, the arrangement of anions and cations results in an octahedral structure comprising one iron atom and six oxygen atoms (Figure 1c).

X-ray diffraction (XRD) patterns obtained experimentally and through simulation were utilized to evaluate the crystal structure of α-Fe_2O_3, as shown in Figure 2. There are 14 characteristic diffraction peaks of α-Fe_2O_3 obtained experimentally at 2θ angles of 24°, 32°, 35°, 39°, 40°, 43°, 49°, 53°, 57°, 61°, 63°, 69°, 71°, and 74° corresponding to lattice planes (012), (104), (110), (006), (113), (202), (024), (116), (018), (214), (300), (208), (119), and (217), respectively. These peaks coincide with the simulated diffraction peaks and are all in good agreement with JCPDS number 33-0664[28].

The optical properties of α-Fe_2O_3 are illustrated in Figure 3, which shows the light absorption of our sample in the wavelength range from 380 nm to 1000 nm. Clearly, the absorption peak is found ca. 400 nm (Figure 3a). A further analysis using Tauc's plot (Figure 3b) revealed that the optical bandgap of our iron oxide material was approximately 2.2 eV, which is similar to the band gap values of α-Fe_2O_3 in other reports[29]. Additionally, the bandgap energy (E_g) is calculated to be approximately 2.2 eV using the Kubelka–Munk equation[30]:

$$(\alpha hv)^n = A\left(hv - E_g\right)$$

where A is a constant, hv is the intensity of the incident light, α is the absorption coefficient, and n is 1/2 for the indirect bandgap and 2 for the direct bandgap.

Figure 4a-c displays SEM images of α-Fe_2O_3 nanorods synthesized at different hydrothermal times (3 h, 4 h, and 5 h). At a hydrothermal duration of 3 hours, the nanorods are still in the early stages of development, exhibiting a fragmented distribution. Conversely, the samples treated for 4 and 5 hours had nanorods with consistent density and well-defined structures. However, considering the time and energy efficiency, the 4-hour hydrothermal sample was selected as the most suitable sample for further investigation. Subsequently, SEM analysis at a scale of 1 μm (Figure 4d) revealed uniform growth of nanorods across a substantial area. Additionally, EDX analysis (Figure 4e) detected Fe, O, Si, and C elements without any presence of any foreign elements, further confirming the high purity of the synthesized sample.

Figure 5 shows the Raman spectrum of the α-Fe_2O_3 nanorods. Apart from the characteristic peak of the silicon substrate at 521 cm^{-1}, the remaining peaks are indicative of the hematite structure[31,32]. Specifically, the peaks at 224 and 475 cm^{-1} are assigned to the A_{1g} vibrational mode, while the five peaks at approximately 244, 291, 408, 609, and 814 cm^{-1} are attributed to the E_g mode.

Figure 6a and Figure 6b depict the absorption spectra of the MB solution in the absence and presence of α-Fe_2O_3 NRs under visible light, respectively. Throughout the dark stirring process, the maximum absorption intensity of the MB solution containing the α-Fe_2O_3 NRs gradually decreased, indicating that MB adsorbed onto the stable material surface. Upon illumination, the intensity of the absorption peak of the MB solution with the α-Fe_2O_3 NRs catalyst decreased more rapidly over time than that of the solution without the catalyst. This observation proves that the α-Fe_2O_3 NRs material exhibits photocatalytic activity in the visible light region. Hence, to further assess the photocatalytic performance, the degradation efficiency and reaction rate constant of MB by the α-Fe_2O_3 NRs were calculated (Figure 7).

DISCUSSION

The VESTA simulation findings for the crystal structure of α-Fe_2O_3 (Figure 1) reveal that the hematite structure is based on the arrangement of O^{2-} anions, which form a hexagonal close-packed (HCP) lattice along the [001] direction of the Fe^{3+} cations. One iron atom and six oxygen atoms form an octahedral unit, with each octahedral unit sharing edges with three neighboring octahedra in the same plane. Consequently, the octahedral units undergo distortion, resulting in two different bond lengths of Fe–O, measured at 1.98 Å and 2.09 Å[33]. In the XRD pattern (Figure 2), the experimentally synthesized sample exhibits the presence of 14 characteristic diffraction peaks of α-Fe_2O_3 without any additional peaks, indicating the high purity of the sample obtained through the hydrothermal method in this study. This finding contributes to demonstrating the successful attainment of

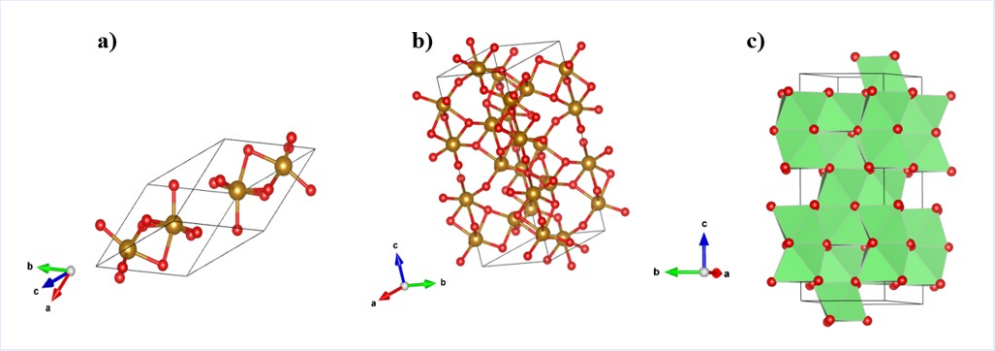

Figure 1: Models for the crystal cell structure of α-Fe_2O_3:**a)** the rhombohedral primitive cell, **b)** the conventional unit cell of α-Fe_2O_3 and **(c)** the octahedral structure in the unit cell. Top of Form

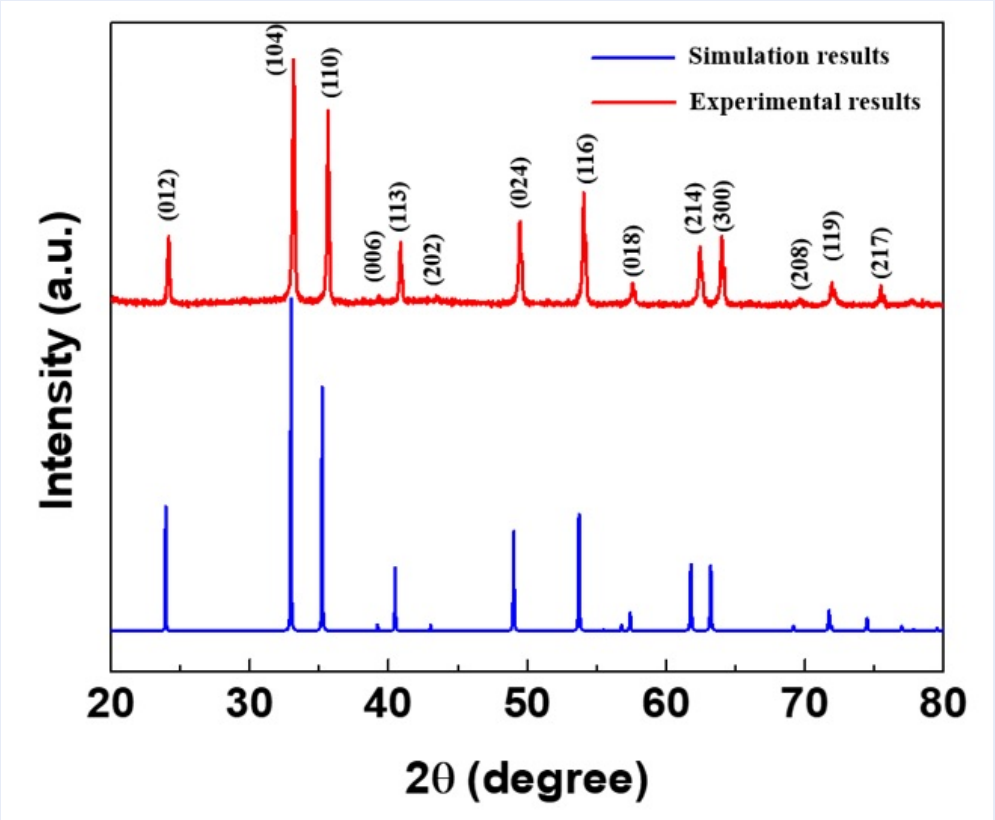

Figure 2: XRD pattern of α-Fe2O3 NRs obtained from the experiment (red line) and from the simulation (blue line)

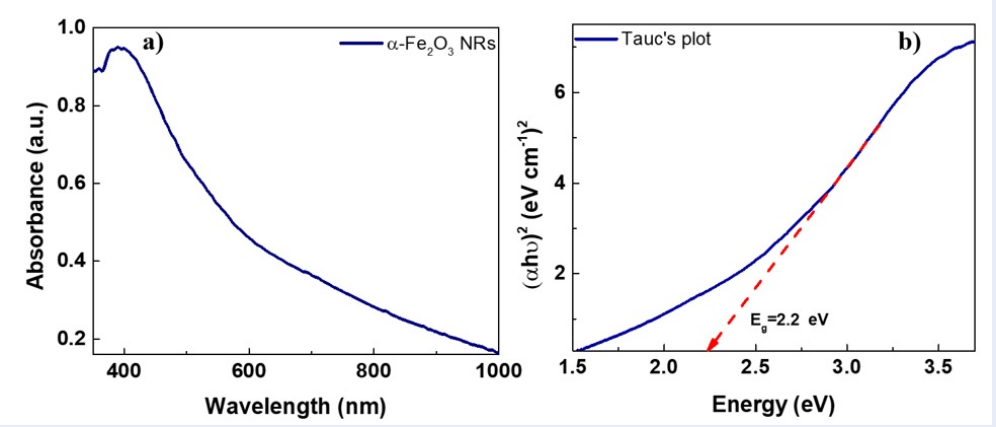

Figure 3: a) UV-Vis absorption spectrum was recorded from the wavelength of 350 to 1000 nm and b) The optical bangapd of the α-Fe2O3 NRs was caculated from Tauc method

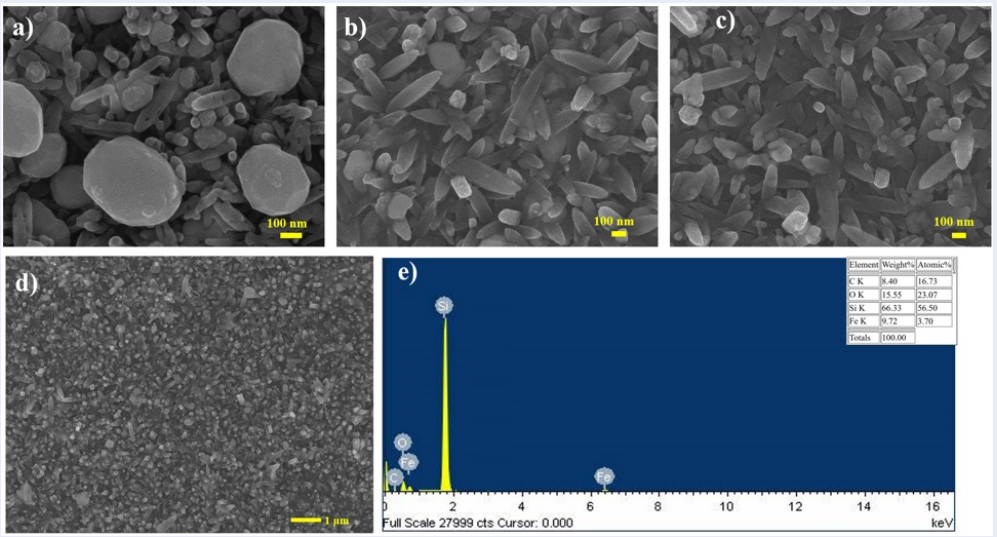

Figure 4: SEM images of α-Fe_2O_3 NRs at different hydrothermal times: a) 3 h, b) 4 h, and c) 5 h. d) Large-scale SEM image and e) EDX spectrum of the α-Fe_2O_3 NRs sample after 4 h of hydrothermal treatment.

the α phase of Fe_2O_3 with the depicted crystal structure. Additionally, the fundamental parameters of the diffraction peaks obtained from the simulation are clearly depicted in Table 1. In the UV–Vis absorption spectrum (Figure 3), the α-Fe_2O_3 NRs exhibit a wide absorption range, with a peak at a wavelength of approximately 400 nm. The optical band gap was calculated at a value of 2.2 eV using Tauc's method. This indicates the suitability of α-Fe_2O_3 NRs for efficient photocatalytic applications under visible light. In addition, nanorods subjected to 4 hours of hydrothermal treatment exhibited uniform growth with high density, with an average diameter of 110 nm and a length of 415 nm (depicted in Figure 4b and Figure 4d). Additionally, the EDX spectrum (Figure 4e) only detected the presence of elements that make up hematite (Fe and O), along with signals from the silicon substrate (Si) and carbon tape (C) utilized during the EDX measurement process. This further underscores the high purity of the prepared sample. Therefore, α-Fe_2O_3 NRs present distinct advantages for applications requiring large surface areas or structured patterns, particularly in the realm of photocatalysis, due to their exceptional adsorption capacity for decomposing organic compounds. In the Raman spectrum of α-Fe_2O_3 depicted in Figure 5, the peaks cor-

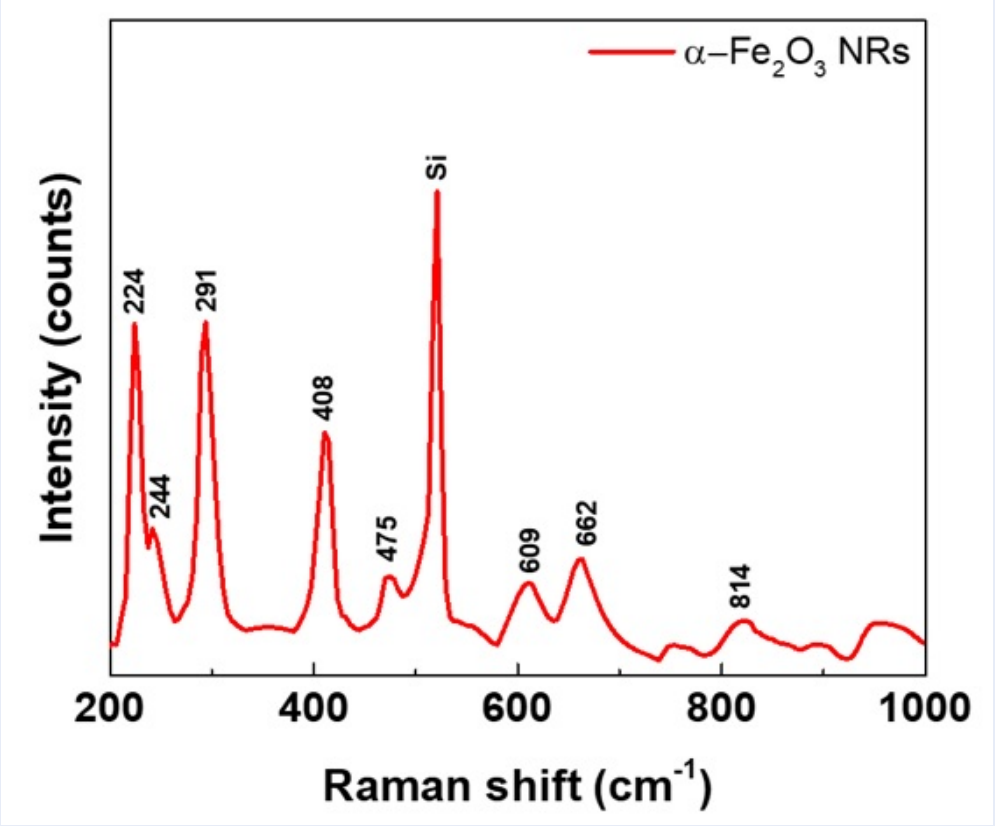

Figure 5: Raman spectrum of the α-Fe_2O_3 NRs under excited laser with the wavelength of 532 nm

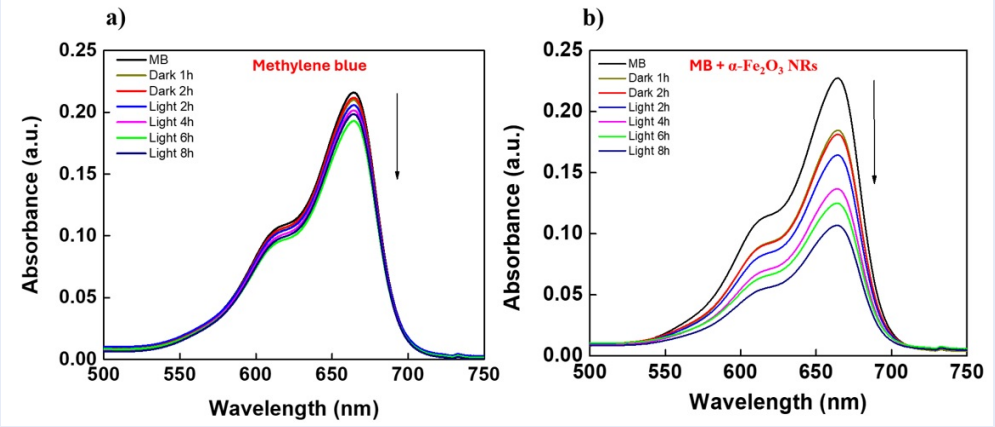

Figure 6: (a) The absorption spectra of methylene blue (MB) without and b) with α-Fe_2O_3 NRs under dark and light conditions

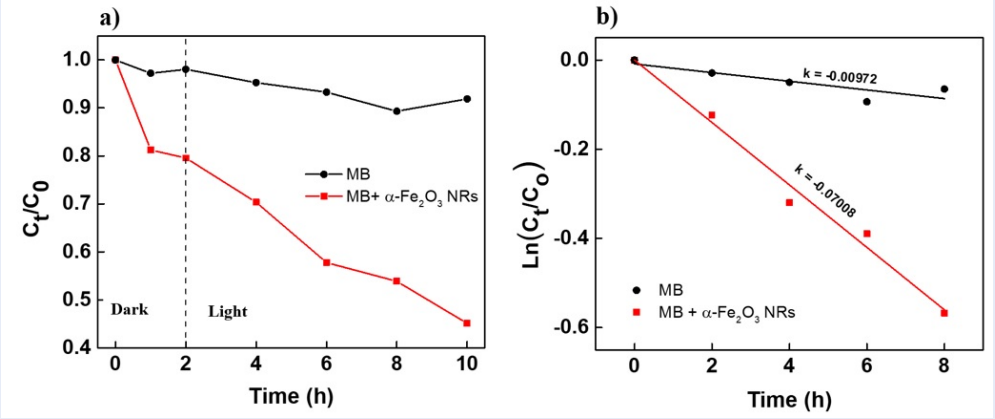

Figure 7: (a) Degradation curve of the MB solution under dark and visible light conditions. (b) The reaction kinetics constant of MB with and without α-Fe_2O_3 NRs.

responding to the A_{1g} vibrational mode at 224 and 475 cm^{-1} indicate symmetric stretching vibrations of the Fe–O bond, while those assigned to the E_g mode at 244, 291, 408, 609, and 814 cm^{-1} represent symmetric bending vibrations of the same bond[7]. Besides, the characteristic peaks of hematite mentioned above, the appearance of vibrations at around 662 cm^{-1} is related to larger nanoparticles than to the size of the nanostructured particles[8,9]. This may explain why this peak is not always observed in the Raman spectra of nanostructured hematite[10]. This result is consistent with the SEM images demonstrating the synthesis of α-Fe_2O_3 as nanorods. Moreover, the detected Raman bands signify the propagation of lattice vibration waves, known as phonons, arising from repetitive and systematic oscillations of the crystal lattice within the hematite structure[11]. Notably, the characteristic vibration peaks of hematite synthesized through this method exhibit high sharpness and clarity. Comparing the Raman spectrum with the XRD pattern (Figure 2) reaffirms the high crystallization of the synthesized hematite structure. Furthermore, apart from the silicon substrate peak at 521 cm^{-1}, no anomalous peaks indicative of parasitic phases, other iron oxides, or iron oxyhydroxides were detected. Moreover, the dye degradation efficiency was calculated using the following equation[12]:

$$\% \text{ dye degradation} = [(C_0 - C_t)/C_0] \times 100\% \quad (1)$$

The photodegradation of these nanomaterials was also quantitatively described using the pseudo-first-order kinetic equation, which is the most common rate law and was adopted as follows[13]:

$$\ln(C_t/C_0) = -kt \quad (2)$$

where C_0 and C_t are the initial dye concentration and dye concentration at time 't', respectively.

The results indicate that in the absence of a catalyst, the self-degradation capacity of MB (2.5 ppm) is only approximately 10%. With the α-Fe_2O_3 NRs catalyst in the MB sample, after adsorption-desorption equilibrium, the MB concentration decreased to 78% of the initial concentration. This reduction corresponds to the removal of approximately 22% of MB due to its absorption onto the material's surface. After 8 h of the photocatalytic reaction, the MB concentration decreased further to 45%, indicating an additional 33% removal through the photocatalytic process. These results demonstrate that 55% of the α-Fe_2O_3 NRs were removedin this study. Furthermore, the reaction rate constant of the MB solution in the presence of the α-Fe_2O_3 NRs catalyst is -0.07008, approximately 7.2 times greater than the rate constant of MB without α-Fe_2O_3 NRs, which is -0.00972. Although the photocatalytic efficiency of α-Fe_2O_3 NRs is not yet high, this material has potential due to the simplicity of the fabrication process and sample recovery after the catalytic reaction.

CONCLUSIONS

In summary, we have successfully synthesized α-Fe_2O_3 nanorods through a simple, rapid, and cost-effective process, yielding promising results. Specifically, nanorods withaverage lengths and diameters of 415 nm and 110 nm, respectively, were grown at a uniform density. Furthermore, the synthesized nanorods exhibited an E_g of 2.2 eV and demonstrated a 55%degradation efficiency of MB throughout the entire process. Additionally, through a combination of experimental and simulation approaches, it has been confirmed that these α-Fe_2O_3 nanorods

Table 1: Basic parameters of the diffraction peaks of α-Fe_2O_3

h	k	l	2θ	d (Å)	h	k	l	2θ	d (Å)
0	1	2	23.942	3.7137	2	1	10	93.019	1.0618
1	0	4	32.976	2.7141	4	0	4	94.388	1.0499
1	1	0	35.223	2.546	1	1	12	94.805	1.0464
0	0	6	39.21	2.2957	1	3	7	95.73	1.0387
1	1	3	40.481	2.2266	3	2	1	99.542	1.0089
2	0	2	43.04	2.0999	1	2	11	100.6	1.0011
0	2	4	49.019	1.8569	2	3	2	100.63	1.0009
1	1	6	53.719	1.7049	3	1	8	101.17	0.9971
2	1	1	55.49	1.6546	2	2	9	103.83	0.9787
1	2	2	56.784	1.62	3	2	4	105.05	0.9706
0	1	8	57.407	1.6039	4	1	0	106.35	0.9623
2	1	4	61.788	1.5002	0	1	14	106.68	0.9603
3	0	0	63.208	1.4699	2	3	5	108.41	0.9497
1	2	5	65.39	1.426	1	4	3	109.75	0.9418
2	0	8	69.17	1.357	4	1	3	109.75	0.9418
1	0	10	71.73	1.3148	0	4	8	112.13	0.9284
1	1	9	71.923	1.3117	1	3	10	114.76	0.9146
2	2	0	74.474	1.273	3	0	12	116.74	0.9047
2	1	7	74.554	1.2718	0	3	12	116.74	0.9047
3	0	6	76.963	1.2379	3	2	7	117.77	0.8997
0	3	6	76.963	1.2379	2	0	14	118.04	0.8985
2	2	3	77.797	1.2267	2	1	13	118.96	0.8942
1	3	1	78.44	1.2182	4	1	6	120.45	0.8875
3	1	2	79.536	1.2042	1	4	6	120.45	0.8875
1	2	8	80.066	1.1975	3	1	11	123.38	0.8749
0	2	10	82.506	1.1682	5	0	2	123.42	0.8748
1	3	4	83.882	1.1525	2	3	8	124.04	0.8722
0	0	12	84.3	1.1479	1	1	15	126.18	0.8638
3	1	5	87.118	1.1178	4	0	10	127.01	0.8607
2	2	6	87.564	1.1133	0	5	4	128.74	0.8544
0	4	2	90.083	1.0886					

possess a rhombohedral crystal structure and belong to the space group $R\bar{3}c$. With this characterization, we hope to provide valuable insights to facilitate further research endeavors based on α-Fe_2O_3 nanorods, thereby expanding the potential applications of this material in the future.

COMPETING INTERESTS

The authors declare that there are no conflicts of interest related to the publication of this article.

AUTHORS' CONTRIBUTIONS

H. N. Luong: carried out the experiment, writing manuscript. **H. N. Luong, L. T. Duy**: measured and analyzed XRD data based on experiments and simulations. **L. N. T. Nguyen, C. K. Tran**: measured, analyzed SEM and UV-Vis data. **H. N. Luong**, **T. M. Dinh, N. D. N. Huynh**: investigated the material's capacity for degrading MB via the photocatalytic process.. **V. Q. Dang**: managed the experiment, collected data to write the paper.

ACKNOWLEDGMENTS

This research is funded by Vietnam National Foundation for Science and Technology Development (NAFOSTED) under grant number 103.03-2021.59.

REFERENCES

1. Iijima S. Helical microtubules of graphitic carbon. Nature 1991; 354: 56-58;Available from: https://doi.org/10.1038/354056a0.
2. Hsu C-Y, Rheima AM, Abbas Z sabri, Faryad MU, Kadhim MM, Altimari US et al. Nanowires Properties and Applications: A Review Study. South African Journal of Chemical Engineering 2023; 46: 286-311;Available from: https://doi.org/10.1016/j.sajce.2023.08.006.
3. Abdullah M, Kamarudin SK. Titanium dioxide nanotubes (TNT) in energy and environmental applications: An overview. Renewable and Sustainable Energy Reviews 2017; 76: 212-225;Available from: https://doi.org/10.1016/j.rser.2017.01.057.
4. Naidu KCB, Kumar NS, Banerjee P, Reddy BVS. A review on the origin of nanofibers/nanorods structures and applications. J Mater Sci: Mater Med 2021; 32: 68;PMID: 34117944. Available from: https://doi.org/10.1007/s10856-021-06541-7.
5. Sharmin M, Podder J. Band gap tuning, n-type to p-type transition and ferrimagnetic properties of Mg doped α-Fe2O3 nanostructured thin films. Journal of Alloys and Compounds 2020; 818: 152850;Available from: https://doi.org/10.1016/j.jallcom.2019.152850.
6. Arun T, Prabakaran K, Udayabhaskar R, Mangalaraja RV, Akbari-Fakhrabadi A. Carbon decorated octahedral shaped Fe3O4 and α-Fe2O3 magnetic hybrid nanomaterials for next generation supercapacitor applications. Applied Surface Science 2019; 485: 147-157;Available from: https://doi.org/10.1016/j.apsusc.2019.04.177.
7. Tadic M, Kopanja L, Panjan M, Lazovic J, Tadic BV, Stanojevic B et al. Rhombohedron and plate-like hematite (α-Fe2O3) nanoparticles: synthesis, structure, morphology, magnetic properties and potential biomedical applications for MRI. Materials Research Bulletin 2021; 133: 111055;Available from: https://doi.org/10.1016/j.materresbull.2020.111055.
8. Wang X, Wang T, Si G, Li Y, Zhang S, Deng X et al. Oxygen vacancy defects engineering on Ce-doped α-Fe2O3 gas sensor for reducing gases. Sensors and Actuators B: Chemical 2020; 302: 127165;Available from: https://doi.org/10.1016/j.snb.2019.127165.
9. Lv X, Zheng P, Wu Z, Yu J, Ge D, Yang L. Self-assembly of Fe2O3 nanorods in carbon nanotube network as a 3D aerogel architecture for lithium-ion batteries. Ceramics International 2019; 45: 5796-5800;Available from: https://doi.org/10.1016/j.ceramint.2018.12.047.
10. Gerami SE, Pourmadadi M, Fatoorehchi H, Yazdian F, Rashedi H, Nigjeh MN. Preparation of pH-sensitive chitosan/polyvinylpyrrolidone/α-Fe2O3 nanocomposite for drug delivery application: Emphasis on ameliorating restrictions. International Journal of Biological Macromolecules 2021; 173: 409-420;PMID: 33454326. Available from: https://doi.org/10.1016/j.ijbiomac.2021.01.067.
11. Xiao C, Li J, Zhang G. Synthesis of stable burger-like α-Fe2O3 catalysts: Formation mechanism and excellent photoFenton catalytic performance. Journal of Cleaner Production 2018; 180: 550-559;Available from: https://doi.org/10.1016/j.jclepro.2018.01.127.
12. Alhabradi M, Nundy S, Ghosh A, Tahir AA. Vertically Aligned CdO-Decked α-Fe2O3 Nanorod Arrays by a Radio Frequency Sputtering Method for Enhanced Photocatalytic Applications. ACS Omega 2022; 7: 28396-28407;PMID: 35990474. Available from: https://doi.org/10.1021/acsomega.2c02996.
13. Popov N, Krehula S, Ristić M, Kuzmann E, Homonnay Z, Bošković M et al. Influence of Cr doping on the structural, magnetic, optical and photocatalytic properties of α-Fe2O3 nanorods. Journal of Physics and Chemistry of Solids 2021; 148: 109699;Available from: https://doi.org/10.1016/j.jpcs.2020.109699.
14. Yan X, Wu Y, Li D, Hu J, Li G, Li P et al. Synthesis and evolution of α-Fe2O3 nanorods for enhanced visible-light-driven photocatalysis. J Mater Sci 2018; 53: 15850-15858;Available from: https://doi.org/10.1007/s10853-018-2751-0.
15. Demirci S, Yurddaskal M, Dikici T, Sarıoğlu C. Fabrication and characterization of novel iodine doped hollow and mesoporous hematite (Fe2O3) particles derived from sol-gel method and their photocatalytic performances. Journal of Hazardous Materials 2018; 345: 27-37;PMID: 29128724. Available from: https://doi.org/10.1016/j.jhazmat.2017.11.009.
16. Tadic M, Trpkov D, Kopanja L, Vojnovic S, Panjan M. Hydrothermal synthesis of hematite (α-Fe2O3) nanoparticle forms: Synthesis conditions, structure, particle shape analysis, cytotoxicity and magnetic properties. Journal of Alloys and Compounds 2019; 792: 599-609;Available from: https://doi.org/10.1016/j.jallcom.2019.03.414.
17. Wu M-S, Ou Y-H, Lin Y-P. Iron Oxide Nanosheets and Nanoparticles Synthesized by a Facile Single-Step Coprecipitation Method for Lithium-Ion Batteries. J Electrochem Soc 2011; 158: A231;Available from: https://doi.org/10.1149/1.3527982.
18. Khalil AT, Ovais M, Ullah I, Ali M, Shinwari ZK, Maaza M. Biosynthesis of iron oxide (Fe2O3) nanoparticles via aqueous extracts of Sageretia thea (Osbeck.) and their pharmacognostic properties. Green Chemistry Letters and Reviews 2017; 10: 186-201;Available from: https://doi.org/10.1080/17518253.2017.1339831.
19. Ramesh R, Ashok K, Bhalero GM, Ponnusamy S, Muthamizhchelvan C. Synthesis and properties of α-Fe2O3 nanorods. Crystal Research and Technology 2010; 45: 965-968;Available from: https://doi.org/10.1002/crat.201000140.
20. Pradhan GK, Parida KM. Fabrication, Growth Mechanism, and Characterization of α-Fe2O3 Nanorods. ACS Appl Mater Interfaces 2011; 3: 317-323;PMID: 21214197. Available from: https://doi.org/10.1021/am100944b.
21. Zeng S, Tang K, Li T. Controlled synthesis of α-Fe2O3 nanorods and its size-dependent optical absorption, electrochemical, and magnetic properties. Journal of Colloid and Interface Science 2007; 312: 513-521;PMID: 17498731. Available from: https://doi.org/10.1016/j.jcis.2007.03.046.
22. Zhang G-Y, Feng Y, Xu Y-Y, Gao D-Z, Sun Y-Q. Controlled synthesis of mesoporous α-Fe2O3 nanorods and visible

light photocatalytic property. Materials Research Bulletin 2012; 47: 625-630;Available from: https://doi.org/10.1016/j.materresbull.2011.12.032.
23. Shi Y, Li H, Wang L, Shen W, Chen H. Novel α-Fe2O3/CdS Cornlike Nanorods with Enhanced Photocatalytic Performance. ACS Appl Mater Interfaces 2012; 4: 4800-4806;PMID: 22894770. Available from: https://doi.org/10.1021/am3011516.
24. Pradhan GK, Padhi DK, Parida KM. Fabrication of α-Fe2O3 Nanorod/RGO Composite: A Novel Hybrid Photocatalyst for Phenol Degradation. ACS Appl Mater Interfaces 2013; 5: 9101-9110;PMID: 23962068. Available from: https://doi.org/10.1021/am402487h.
25. Chen D, Liu Z. Dual-Axial Gradient Doping (Zr and Sn) on Hematite for Promoting Charge Separation in Photoelectrochemical Water Splitting. ChemSusChem 2018; 11: 3438-3448;PMID: 30098118. Available from: https://doi.org/10.1002/cssc.201801614.
26. Dzade NY, Roldan A, De Leeuw NH. A Density Functional Theory Study of the Adsorption of Benzene on Hematite (α-Fe2O3) Surfaces. Minerals 2014; 4: 89-115;Available from: https://doi.org/10.3390/min4010089.
27. Gedamu Tamirat A, Rick J, Aregahegn Dubale A, Su W-N, Hwang B-J. Using hematite for photoelectrochemical water splitting: a review of current progress and challenges. Nanoscale Horizons 2016; 1: 243-267;PMID: 32260645. Available from: https://doi.org/10.1039/C5NH00098J.
28. Rao X, Su X, Yang C, Wang J, Zhen X, Ling D. From spindle-like β-FeOOH nanoparticles to α-Fe2O3 polyhedral crystals: shape evolution, growth mechanism and gas sensing property. CrystEngComm 2013; 15: 7250-7256;Available from: https://doi.org/10.1039/c3ce40430g.
29. Li F, Li J, Zhang J, Gao L, Long X, Hu Y et al. NiO Nanoparticles Anchored on Phosphorus-Doped α-Fe2O3 Nanoarrays: An Efficient Hole Extraction p-n Heterojunction Photoanode for Water Oxidation. ChemSusChem 2018; 11: 2156-2164;PMID: 29768719. Available from: https://doi.org/10.1002/cssc.201800571.
30. Su J, Feng X, Sloppy JD, Guo L, Grimes CA. Vertically Aligned WO3 Nanowire Arrays Grown Directly on Transparent Conducting Oxide Coated Glass: Synthesis and Photoelectrochemical Properties. Nano Lett 2011; 11: 203-208;PMID: 21114333. Available from: https://doi.org/10.1021/nl1034573.
31. Wei Q, Zhang Z, Li Z, Zhou Q, Zhu Y. Enhanced photocatalytic activity of porous α-Fe2O3 films prepared by rapid thermal oxidation. J Phys D: Appl Phys 2008; 41: 202002;Available from: https://doi.org/10.1088/0022-3727/41/20/202002.
32. Bulin C, Li B, Zhang Y, Zhang B. Removal performance and mechanism of nano α-Fe2O3/graphene oxide on aqueous Cr(VI). Journal of Physics and Chemistry of Solids 2020; 147: 109659;Available from: https://doi.org/10.1016/j.jpcs.2020.109659.
33. Naveas N, Pulido R, Marini C, Hernández-Montelongo J, Silván MM. First-principles calculations of hematite (α-Fe2O3) by self-consistent DFT+U+V. iScience 2023; 26: 106033;PMID: 36824287. Available from: https://doi.org/10.1016/j.isci.2023.106033.